Vesiculation mechanisms mediated by anisotropic proteins

Ke Xiao

Department of Physics, College of Physical Science and Technology, Xiamen University, Xiamen 361005, People's Republic of China and Wenzhou Institute, University of Chinese Academy of Sciences, Wenzhou 325016, People's Republic of China

Chen-Xu Wu* and Rui Ma†

Department of Physics and Fujian Provincial Key Laboratory for Soft Functional Materials Research, College of Physical Science and Technology, Xiamen University, Xiamen 361005, People's Republic of China

(Received 10 November 2022; accepted 24 April 2023; published 20 June 2023)

Endocytosis is an essential biological process for the trafficking of macromolecules in cells. In yeast cells, this involves the invagination of a tubular membrane and the formation of endocytic vesicles. The crescent-shaped BAR proteins are generally assumed to squeeze the tubular membrane and pinch off the vesicle. Here, we theoretically investigate how BAR proteins help drive membrane fission via generating anisotropic curvatures. We show that increasing the isotropic spontaneous curvature at a localized region on the side of a tubular membrane cannot induce membrane fission if the coating area is small. However, a tubular membrane coated with proteins that generate anisotropic curvatures are prone to experience an hourglass-shaped or tube-shaped necking process, which leads to membrane fission. In addition, we propose an experimental method to determine the type of anisotropic curvatures of a protein.

DOI: 10.1103/PhysRevResearch.5.023176

I. INTRODUCTION

Endocytosis is involved in many cellular processes, including nutrient uptake, regulated recycling of plasma membrane components, and neural signaling [1]. This process is achieved through formation of transient, highly curved membrane configurations such as tubules or vesicles, which have the targeted molecules wrapped inside [2]. During endocytosis in yeast cells, a small patch of the plasma membrane is first deformed into a shallow invagination, which is subsequently elongated into a deep one, followed by a constriction of its neck until a cargo-carrying vesicle is formed and pinched off [3].

These membrane-shaping events are generally mediated by a plethora of types of proteins bound to the membrane [4–7]. Clathrin proteins play an important role. They can assemble into a polyhedral lattice with a mixture of pentagons and hexagons that tends to fold into a basketlike structure. The rigid basket scaffolds the flat membrane into a spherical pit [8–11]. After formation of the pit, the GTPase dynamin proteins can form a helical band at the neck of the endocytic pit. In mammalian cells, it is generally thought that the constriction of the band upon GTP hydrolysis drives vesicle scission. Other active participants to facilitate vesicle scission are the Bin/amphiphysin/Rvs (BAR) domain proteins that are found to be bound at the side of the endocytic pit and assemble into a cylindrical scaffold. The crescent-shaped BAR proteins are expected to bend the membrane into different curvatures in parallel with and perpendicular to their orientations [3,12–14]. Such a mechanical feature, enhanced by the enrichment of BAR proteins on the membrane, can induce tubulation [15–17]. The role of BAR proteins as facilitators for vesicle scission has been challenged by Walani *et al.* [18], who proposed that the BAR proteins help stabilize the tubular endocytic pit, and it is the depolymerization of BAR proteins that leads to the scission of the tubular pit through a snap-through transition induced by high membrane tension.

Membrane budding and vesiculation have been extensively studied, both in theory and in experiments [19–24]. In the case of a homogeneous membrane, excessive surface area–to–volume ratio could lead to formation of a pear-shaped membrane where a small vesicle buds from a large vesicle, or a pearl-shaped membrane where multiple equal-sized vesicles are connected in series. The neck connecting the vesicles in theory can be infinitely narrow but does not contribute to the bending energy [25–27]. Line tension developed at the interface between two intramembrane domains could also lead to an infinitesimal neck [28,29]. However, the presence of various types of proteins in different locations on the membrane during endocytosis gives rise to heterogeneity in mechanical properties of the membrane, such as the bending rigidity [30] and the membrane curvature [31]. The physical mechanisms behind membrane vesiculation during endocytosis, which is a highly heterogenous system, remains unclear.

Rapid developments in imaging technologies such as electron and fluorescence microscopy have resolved the shapes of

*cxwu@xmu.edu.cn
†ruima@xmu.edu.cn

the endocytic pit at different stages of endocytosis [32–34]. Experiments have confirmed that vesicle formation can arise from the conical shape of lipid molecules [35,36], membrane tension induced by external forces [37–39], as well as spontaneous curvature generated by membrane-bound proteins [40–43]. Theoretical efforts were also exploited to interpret the underlying mechanical principles of membrane-budding phenomena during endocytosis [18,44–48]. Most of these works focus on the explanation of how a flat membrane is deformed into either a tubular pit via external forces or a spherical vesicle via clathrin assembly. The very last step of vesicle scission has been studied only in a limited number of works. By constructing a quantitative model, Liu *et al.* [45] suggested that the line tension at the interface between different lipid domains on the invaginating membrane is sufficient for a successful vesicle scission during endocytosis. The inhomogeneity of the membrane arises from enrichment of proteins on a localized area as a result of phase separation [21–23]. However, experimental evidence for lipid phase separation on the endocytic pit is still lacking.

In the classical Helfrich model of membrane, the effect of curvature generation by proteins on the membrane is embedded in a parameter called *spontaneous curvature*. To reduce the energetic cost for bending, the membrane tends to deform in such a way that the mean curvature of the membrane equals the spontaneous curvature. However, this description of curvature generation cannot capture the effect of anisotropic proteins, such as BAR proteins, which tend to bend the membrane independently into different curvatures in different tangential directions. Whether the anisotropic curvature generated by BAR proteins at the side of a tubular membrane can induce vesicle scission remains unclear.

In this paper, using the extended Helfrich model developed to account for the anisotropic spontaneous curvatures generated by anisotropic proteins [49–52], we investigate how a tubular membrane is deformed by anisotropic proteins bound to the side of the membrane. It is found that, within the classical Helfrich model of a membrane, increasing the spontaneous curvature cannot lead to membrane fission if the coating area of proteins is small. Anisotropic spontaneous curvatures are necessary to narrow the membrane into a tubular neck or an hourglass neck. We also suggest an experimental method to distinguish the type of anisotropic spontaneous curvatures generated by a protein by comparing the force to maintain the membrane in a tubular shape in the presence and absence of the protein coat.

II. MODELING ENDOCYTIC INVAGINATION AND ANISOTROPIC PROTEINS

We consider the deformation of a tubular invagination in the late stage of endocytosis in yeast cells when BAR proteins are present at the side of the tube, as shown in Figs. 1(a) and 1(b). The shape of the membrane invagination is assumed to be rotationally symmetric, and the membrane profile is parameterized by the meridional coordinates $[r(s), z(s)]$, where s denotes the arc length from the membrane tip ($s = 0$). We introduce the angle ψ spanned between the tangential direction and the radial horizon, as shown in Fig. 2. With these coordinates, the two principal curvatures of the membrane

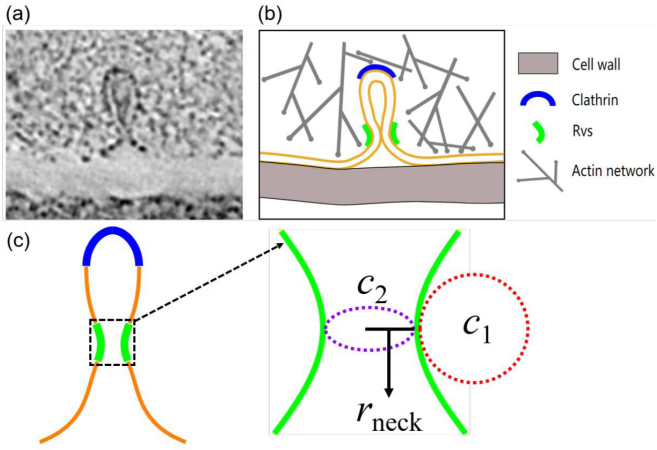

FIG. 1. (a) Electron micrograph of an endocytic invagination in yeast cells when BAR proteins are present. The graph is adapted from Ref. [1]. (b) Schematic illustration of the proteins involved in endocytosis. The clathrin proteins (blue) are bound to the tip of the membrane and generate an isotropic spontaneous curvature. The BAR proteins (green) are bound to the side of the membrane and expected to generate an anisotropic spontaneous curvature to facilitate membrane fission. (c) Characterization of the neck morphology. The narrow neck formed by BAR proteins (green) is depicted by the neck radius r_{neck} and the two principal curvatures c_1 and c_2.

read

$$c_1 = \frac{d\psi}{ds} \equiv \dot{\psi}, \quad c_2 = \frac{\sin\psi}{r}. \tag{1}$$

Hereafter, the overhead dot indicates the derivative with respect to the arc length s.

The membrane invagination is assumed to be pulled by the actin polymerization force f against the high turgor pressure p inside the cell to a fixed height (Fig. 2). The membrane tension σ is assumed to be small due to the presence of eisosomes which serve as a membrane reservoir. To describe the anisotropic spontaneous curvature induced by BAR proteins and the isotropic spontaneous curvature induced by clathrin proteins, we adopt the extended Helfrich model proposed by

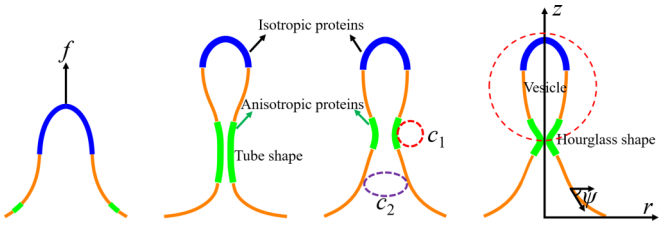

FIG. 2. Schematic picture of the theoretical model for a heterogeneous membrane during endocytosis. We assume a point force f, which is thought to be provided by actin polymerization, is applied at the tip of the membrane patch to maintain the membrane at a fixed height. The clathrin protein-coated area (blue) generates an isotropic spontaneous curvature. The BAR protein-coated area (green) generates an anisotropic spontaneous curvature. Depending on the coupling constant κ_{12}, the membrane tube undergoes a tubular necking or an hourglass necking at the BAR protein-coated area (green).

Walani *et al.* [52], in which the bending energy density of the membrane per unit area is written as

$$f_b = \frac{\kappa}{2}\left(c_1 - c_0^1\right)^2 + \frac{\kappa}{2}\left(c_2 - c_0^2\right)^2 + \kappa_{12}\left(c_1 - c_0^1\right)\left(c_2 - c_0^2\right), \tag{2}$$

where κ denotes the bending rigidity, and c_0^1 and c_0^2 denote the preferred curvature in the longitudinal and circumferential directions, respectively. The coupling constant κ_{12} in general deviates from κ, corresponding to an anisotropic curvature model. When $\kappa_{12} = \kappa$, it reduces to the classical Helfrich model:

$$f_h = \frac{\kappa}{2}\left(c_1 + c_2 - c_0^1 - c_0^2\right)^2. \tag{3}$$

To describe the inhomogeneity of the membrane, the parameters $\kappa(a)$, $\kappa_{12}(a)$, $c_1^0(a)$, and $c_2^0(a)$ are spatially varied as a function of the area $a(s)$ calculated from the membrane tip. At the clathrin-coated area ($a < a_{01}$, blue region in Fig. 2), the coupling constant $\kappa_{12} = \kappa$. The spontaneous curvatures $c_0^1 = c_0^2 = C_{\rm cla}$ take a positive value of $C_{\rm cla} = 0.028\,{\rm nm}^{-1}$. At the BAR protein-coated area ($a_{02} < a < a_{03}$, green region in Fig. 2), the coupling constant κ_{12} deviates from κ in a way of $\kappa_{12} = \kappa + \Delta\kappa$. The spontaneous curvature c_0^1 is fixed at $0\,{\rm nm}^{-1}$, while $c_0^2 = C_{\rm bar}$ is varied from -0.2 to $0.2\,{\rm nm}^{-1}$ to see how the anisotropic curvatures shape the membrane morphology. In the uncoated area of the membrane ($a_{01} < a < a_{02}$ and $a > a_{03}$, orange region in Fig. 2), all spontaneous curvatures c_0^1 and c_0^2 vanish, and $\kappa_{12} = \kappa$. In practice, we have the following spatially varied material property parameters, including the spontaneous curvatures:

$$c_0^1(a) = \tfrac{1}{2}C_{\rm cla}\{1 - \tanh[A_{\rm s}(a - a_{01})]\}, \tag{4}$$

and

$$c_0^2(a) = \tfrac{1}{2}C_{\rm cla}\{1 - \tanh[A_{\rm s}(a - a_{01})]\} + \tfrac{1}{2}C_{\rm bar}\{\tanh[A_{\rm s}(a_{03} - a)] - \tanh[A_{\rm s}(a_{02} - a)]\}, \tag{5}$$

where a_{01} denotes the coating area of clathrin proteins which generate an isotropic spontaneous curvature of $C_{\rm cla}$, $A_{\rm coating} = a_{03} - a_{02}$ denotes the coating area of the BAR proteins which generate an anisotropic spontaneous curvature of $C_{\rm bar}$ in the circumferential direction, and a_{02} indicates the starting position of the BAR proteins. The parameter $A_{\rm s}$ controls the sharpness of the coating edge. Similarly, the bending rigidity varies as

$$\kappa(a) = \kappa_0 + \tfrac{1}{2}\kappa_{\rm cla}\{1 - \tanh[A_{\rm s}(a - a_{01})]\} + \tfrac{1}{2}\kappa_{\rm bar}\{\tanh[A_{\rm s}(a_{03} - a)] - \tanh[A_{\rm s}(a_{02} - a)]\}, \tag{6}$$

where κ_0 denotes the bending rigidity of the uncoated membrane, and $\kappa_{\rm cla}/\kappa_{\rm bar}$ denotes the increment of the bending rigidity due to clathrin/BAR protein coating. The coupling constant

$$\kappa_{12}(a) = \kappa_0 + \tfrac{1}{2}\kappa_{\rm cla}\{1 - \tanh[A_{\rm s}(a - a_{01})]\} + \tfrac{1}{2}\Delta\kappa\{\tanh[A_{\rm s}(a_{03} - a)] - \tanh[A_{\rm s}(a_{02} - a)]\}. \tag{7}$$

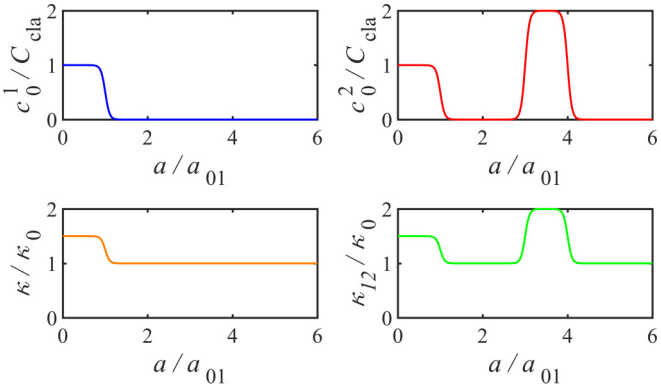

FIG. 3. Illustration of the spatially varied parameters $c_0^1(a)$, $c_0^2(a)$, $\kappa(a)$, and $\kappa_{12}(a)$ as a function of the area a. For the purpose of illustration, here, we set $C_{\rm bar} = 2C_{\rm cla}$, $a_{02} = 3a_{01}$, $a_{03} = 4a_{01}$, $\kappa_{\rm cla} = 0.5\kappa_0$, $\kappa_{\rm bar} = 0\kappa_0$, and $\Delta\kappa = \kappa_0$.

In the BAR protein-coated area $a_{02} < a < a_{03}$, $\Delta\kappa$ deviates from $\kappa_{\rm bar}$. The dependence of $c_0^1(a)$, $c_0^2(a)$, $\kappa(a)$, and $\kappa_{12}(a)$ on area a is shown in Fig. 3.

The bending energy of the membrane reads

$$G_{\rm b} = 2\pi\int_0^S f_b r\,ds, \tag{8}$$

where the integral is taken over the entire surface, with $s = S$ indicating the point at which the membrane is in contact with the cell wall. The total energy of the membrane also has a contribution from the turgor pressure p, which reads

$$G_{\rm p} = pV = 2\pi\int_0^S \frac{1}{2}pr^2\sin\psi\,ds, \tag{9}$$

and from the external force f:

$$G_{\rm f} = -fL = -2\pi\int_0^S \frac{f}{2\pi}\sin\psi\,ds. \tag{10}$$

In addition, we introduce three Lagrangian multipliers to impose the geometric constraints:

$$G_{\rm c} = 2\pi\int_0^S [\alpha(\dot r - \cos\psi) + \beta(\dot z + \sin\psi) + \lambda(\dot a - r)]\,ds. \tag{11}$$

Note that the Lagrangian multiplier $-\lambda$ happens to be the membrane tension. The total energy of the membrane then reads

$$\begin{aligned} G_{\rm tot}[\psi, \dot\psi, r, \dot r, z, \dot z, a, \dot a, \alpha, \beta, \lambda] &= G_{\rm b} + G_{\rm p} + G_{\rm f} + G_{\rm c} \\ &= 2\pi\int_0^S \mathcal{L}[\psi, \dot\psi, r, \dot r, z, \dot z, a, \dot a, \alpha, \beta, \lambda]ds. \end{aligned} \tag{12}$$

To derive the shape equations that govern the morphology of the membrane surface of the endocytic invagination, Euler-Lagrange variational methods were performed on the total free energy of the membrane in Eq. (12) with respect to the shape variables. The detailed derivations of the shape equations are presented in Appendix A. We numerically solve the shape equations in MATLAB using the bvp4c solver, which

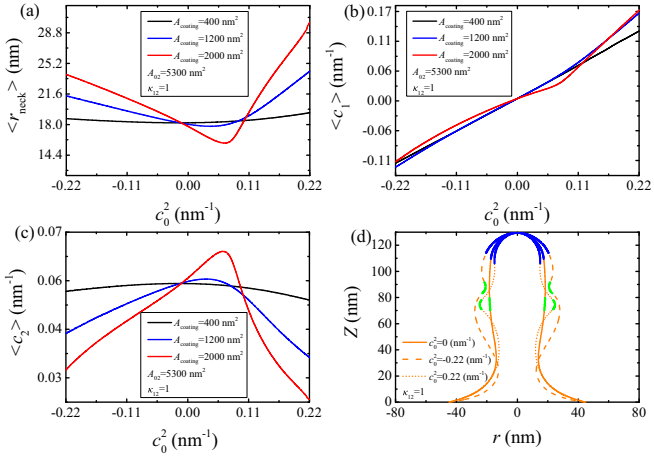

FIG. 4. (a) The mean value of the neck radius $\langle r_{\rm neck}\rangle$ and the two principal curvatures (b) $\langle c_1\rangle$ and (c) $\langle c_2\rangle$, as a function of the spontaneous curvature c_0^2 for the Helfrich model $\kappa_{12}=\kappa$. The average is taken over the protein-coated area at the side of the membrane. The three curves in (a)–(c) correspond to different coating areas. (d) Profile views of membrane morphologies for positive (dotted line), negative (dashed line), and zero (solid line) spontaneous curvature c_0^2.

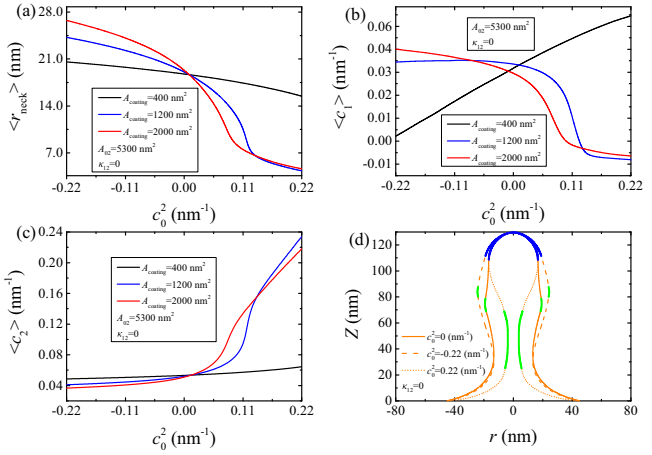

FIG. 5. (a) The mean value of the neck radius $\langle r_{\rm neck}\rangle$ and the two principal curvatures (b) $\langle c_1\rangle$ and (c) $\langle c_2\rangle$, as a function of the spontaneous curvature c_0^2 for $\kappa_{12}=0$. The average is taken over the protein-coated area at the side of the membrane. The three curves in (a)–(c) correspond to different coating areas. (d) Profile views of membrane morphologies for positive (dotted line), negative (dashed line), and zero (solid line) spontaneous curvature c_0^2.

is designed to solve the boundary value problems of ordinary differential equations.

In this paper, we are particularly interested in the morphology of the membrane in the BAR protein-coated area, which is referred to as a neck in the rest of the paper. By choosing different $\kappa_{12}=\kappa_0+\Delta\kappa$, which represent different types of anisotropic spontaneous curvatures, we vary the parameter $c_0^2=C_{\rm bar}$ in the neck and observe the morphology change, which is characterized by the mean neck radius $\langle r_{\rm neck}\rangle$ and the mean of two principal curvatures $\langle c_1\rangle$ and $\langle c_2\rangle$ over the area range $a_{02}<a<a_{03}$. Vesiculation is indicated by reducing the narrowest neck radius <5 nm, a typical critical value conventionally set in previous works [45,47], though we can reduce the neck radius far <5 nm in theory.

III. RESULTS

A. Isotropic spontaneous curvature cannot produce vesiculation if the coating area is small

We first study the case $\kappa_{12}=\kappa$ in the neck. In this case, the model is essentially the classical Helfrich model ($\kappa_{12}=\kappa$), and varying c_0^2 is equivalent to tuning the spontaneous curvature of the Helfrich model. It is shown that the average neck radius $\langle r_{\rm neck}\rangle$ is a nonmonotonic function of c_0^2 with a minimum of $\sim$14 nm, far from the critical value for vesiculation to occur (5 nm) [see Fig. 4(a)]. The average longitudinal curvature $\langle c_1\rangle$ increases with c_0^2 and changes its sign when c_0^2 crosses 0 [Fig. 4(b)], while the average circumferential curvature $\langle c_2\rangle$ reaches a peak value at an intermediate value of c_0^2 [see Fig. 4(c)]. Membrane shapes of positive, negative, and zero spontaneous curvatures c_0^2 are depicted in Fig. 4(d), where the protein-coated area of positive/negative spontaneous curvatures shows a wider radius than that of zero spontaneous curvature. These results suggest that increasing the spontaneous curvature in the Helfrich model cannot produce vesiculation if the coating area of proteins is relatively small ($<2000\,{\rm nm}^2$). When the coating area is large ($>2200\,{\rm nm}^2$), we find that the original Helfrich model can also form a pearl-shaped neck with the narrowest radius <5 nm (see Appendix B). This fission mechanism is essentially due to the excessive coating area of the proteins such that the membrane tends to be shaped into multiple spheres connected by necks with a mean curvature equal to the spontaneous curvature, which has been extensively studied [26,27]. For the rest of the paper, we will limit our discussion to the case where the coating area of proteins is $<2000\,{\rm nm}^2$ and investigate if anisotropic curvature ($\kappa_{12}\neq\kappa$) can induce membrane fission.

B. Anisotropic spontaneous curvature with $\kappa_{12}=0$ produces tubular necking

As a first attempt to study the anisotropic spontaneous curvature with $\kappa_{12}\neq\kappa$, we consider the case $\kappa_{12}=0$. If the area of the anisotropic protein-coated membrane is small, the average neck radius $\langle r_{\rm neck}\rangle$ and the average circumferential curvature $\langle c_2\rangle$ are almost independent of c_0^2 [see black curves in Figs. 5(a) and 5(c)], while the average longitudinal curvature $\langle c_1\rangle$ increases with c_0^2 in a considerable way [see the black curve in Fig. 5(b)]. In contrast, for larger coating area, $\langle r_{\rm neck}\rangle$ is narrowed down with the increase of c_0^2, and the longitudinal curvature $\langle c_1\rangle$ drops to a value that is close to zero [see blue and red curves in Figs. 5(a) and 5(b)], corresponding to a membrane morphology classified as a tubular neck, as depicted by the dotted profile in Fig. 5(d). These results suggest that the extended Helfrich model $\kappa_{12}=0$ can produce vesiculation if the coating area is large enough.

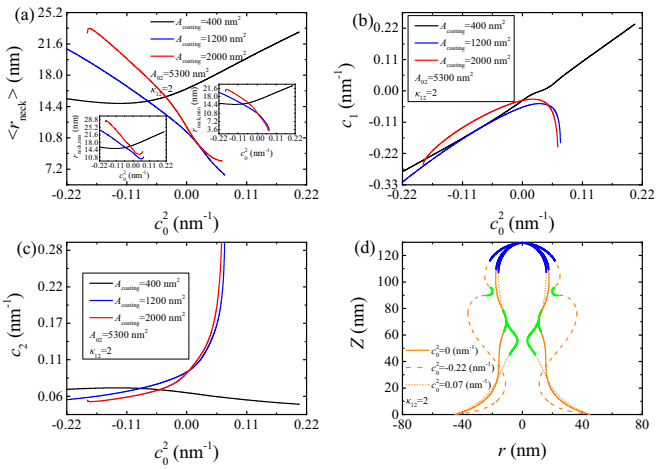

FIG. 6. (a) The mean value of the neck radius $\langle r_{\rm neck}\rangle$ and the two principal curvatures (b) $\langle c_1\rangle$ and (c) $\langle c_2\rangle$, as a function of the spontaneous curvature c_0^2 for $\kappa_{12} = 2\kappa$. The average is taken over the protein-coated area at the side of the membrane. The three curves in (a)–(c) correspond to different coating areas. (d) Profile views of membrane morphologies for positive (dotted line), negative (dashed line), and zero (solid line) spontaneous curvature c_0^2.

C. Anisotropic spontaneous curvature with $\kappa_{12} = 2\kappa$ produces hourglass necking

Subsequently, we consider the anisotropic spontaneous curvature with $\kappa_{12} = 2\kappa$. As the coating area exceeds a certain value, the average neck radius $\langle r_{\rm neck}\rangle$ decreases monotonically with the spontaneous curvature c_0^2. The minimum neck radius $r_{\rm neck,min}$ drops to a few nanometers, indicating the occurrence of vesiculation [see blue and red curves in the inset of Fig. 6(a)]. The morphology of the membrane in this situation corresponds to an hourglass-shaped neck [see the dotted profile in Fig. 6(d)], which is reflected in the large magnitude of principal curvatures c_1 and c_2 with opposite signs [see red and blue curves in Figs. 6(b) and 6(c)].

D. Phase diagram of the neck morphology

To systematically investigate how membrane morphology depends on the coupling constant κ_{12}, we construct a κ_{12}-c_0^2 phase diagram (Fig. 7) summarizing the possible membrane morphologies. For negative and small positive values of κ_{12}, increasing the spontaneous curvature c_0^2 to a critical value leads to vesiculation with a tube-shaped neck (see the black curve encompassing the white region in the top-left corner of Fig. 7). For large positive values of κ_{12}, vesiculation with an hourglass-shaped neck can occur if the spontaneous curvature c_0^2 is beyond a critical value (see the black curve encompassing the white region in the top-right corner of Fig. 7). There exists an intermediate range of κ_{12} in which vesiculation does not occur even for very large c_0^2.

E. A possible experiment to determine the type of anisotropic spontaneous curvature

So far, we have shown that the coupling constant κ_{12} neglected in most previous studies plays an important role in determining whether the anisotropic proteins at the side of the

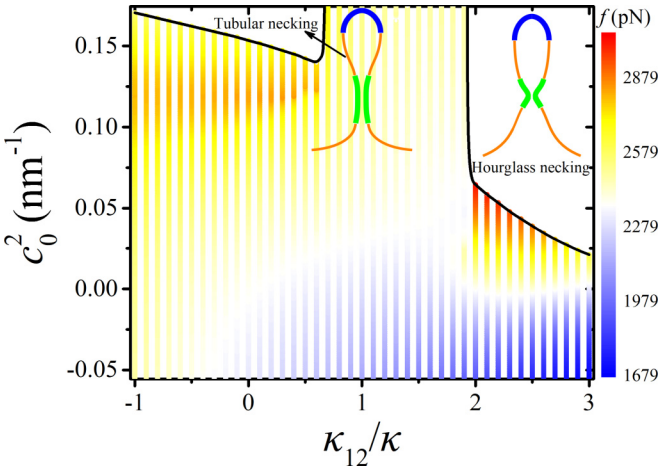

FIG. 7. A two-dimensional phase diagram on the (c_0^2-κ_{12}) plane characterizes the interrelated effects of the spontaneous curvature c_0^2 and the coupling constant κ_{12} on the formation of vesicles. The colored region represents the membrane shapes that have not undergone vesiculation with a color code demonstrating the force magnitude to maintain the membrane at a tubular shape. The white regions represent the membrane shapes that have a necking radius smaller than the critical value of 5 nm, by which a vesiculation is regarded to occur. The top-left corner denotes tube-shaped necking, and the top-right corner denotes hourglass-shaped necking. The coating area $A_{\rm coat}$ is 1200 nm^2.

tubular membrane can drive membrane fission and generate the morphology of the membrane neck if fission occurs. Here, we propose an experimental method to estimate the value of κ_{12}. It should be noted that, to maintain the membrane at a tubular shape, a pulling force f is needed to resist the membrane from being flatten since the membrane tension tends to straighten the membrane, and the turgor pressure tends to push down the membrane against the cell wall. An investigation on how anisotropic proteins bound to the side of the membrane influences the force f shows that f increases with c_0^2 for the classical Helfrich model [see curves in Fig. 8(a)]. In contrast, for the extended Helfrich model $\kappa_{12} = 0$, the force exhibits a gentle increase followed by a decrease with the increase of c_0^2 [see blue and red curves in Fig. 8(b)]. As for the model $\kappa_{12} = 2\kappa$, a sharp increase in the force f is accompanied with a small increase of the spontaneous curvature c_0^2 [see blue and red curves in Fig. 8(c)]. The colored region in Fig. 7 demonstrates how the force depends on the combination of the

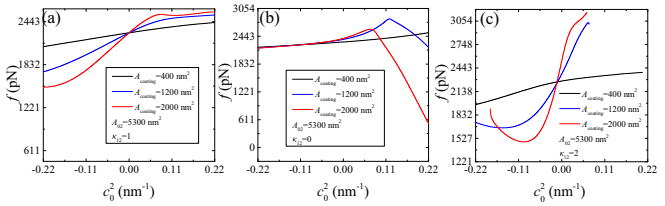

FIG. 8. The dependence of the pulling force f on the spontaneous curvature c_0^2 for different coupling constants (a) $\kappa_{12} = \kappa$, (b) $\kappa_{12} = 0$, and (c) $\kappa_{12} = 2\kappa$. The curves could terminate at certain values of c_0^2 when vesiculation occurs.

coupling constant κ_{12} and the spontaneous curvature c_0^2. In the intermediate range of κ_{12} ($0.7\kappa < \kappa_{12} < 1.9\kappa$), the force f is almost independent of c_0^2. For large κ_{12} ($\kappa_{12} < 0.7\kappa$), the force f has a sharp increase with c_0^2. For small and negative κ_{12} ($\kappa_{12} < 1.9\kappa$), the force f shows a nonmonotonic dependence on c_0^2.

Pulling a membrane tube from a giant liposome with optical tweezers is a common *in vitro* experiment to determine the membrane tension and bending rigidity. When the tube is formed, by flowing the proteins of interest into the solution, the membrane could be gradually bound with the proteins at the lateral side of the tube, and the spontaneous curvature is expected to increase with the enrichment of the proteins. Measuring the force to maintain the membrane at a tubular shape in response to the growth of the protein coat, checking a figure like Fig. 7, and reading how the force depends on the protein concentration, we can estimate the range of the coupling constant for that type of protein.

IV. DISCUSSION

BAR proteins have been proposed as active players in membrane fission during the late stage of endocytosis in yeast cells. The crescent-shaped N-BAR proteins have a typical radius of 10 nm and can induce membrane tubulation of the same radius when the density is high enough [15–17]. We have shown in the phase diagram of Fig. 7 that the coupling constant κ_{12} determines whether membrane fission could happen upon increasing the spontaneous curvature c_0^2. For strong coupling ($\kappa_{12} > 2\kappa$), a small spontaneous curvature c_0^2 ($>0.05\,\mathrm{nm}^{-1}$) generated by the binding of BAR proteins is enough to induce vesiculation. However, for small positive and negative values of κ_{12}, a very large spontaneous curvature c_0^2 ($>0.13\,\mathrm{nm}^{-1}$) is needed to induce vesiculation. As it is known that N-BAR proteins have a curvature of $\approx 0.1\,\mathrm{nm}^{-1}$ ($<0.13\,\mathrm{nm}^{-1}$ but $>0.05\,\mathrm{nm}^{-1}$), our results therefore suggest that N-BAR proteins can actively induce membrane fission not via tubular necking but via hourglass necking. We stress that this conjecture holds only if the coating area of the BAR proteins is small ($<2000\,\mathrm{nm}^2$). To estimate the coating area of BAR proteins in yeast cells, we find that the copy number of Rvs167 is $\sim$100 [53]. They can make up 50 dimers which have a crescent shape that spans a dimension of 10 nm in length and 3 nm in width due to three α-helices, each having a diameter of 1 nm [17]. Assuming they are tightly packed on the surface of the membrane, the coating area therefore is $\sim 1500\,\mathrm{nm}^2$. On the other hand, we might underestimate the coating area if the BAR proteins are loosely packed.

As a result of the high turgor pressure inside yeast cells, maintaining the membrane in a tubular shape requires a very large force. Actin polymerization is assumed to provide the force. However, based on the copy number analysis of actin filaments, polymerization alone seems unable to generate enough force [48,54]. We have found that anisotropic proteins with a coupling constant $\kappa_{12} = 0$ could significantly reduce the force to maintain the membrane at a tubular shape from 2000 to 600 pN. This result provides a perspective to explain the large difference between the required force and the actual force generated by actin polymerization.

V. CONCLUSIONS

In summary, we study the physics behind vesiculation phenomena via anisotropic proteins bound to the side of a tubular membrane during endocytosis. It is found that the classical Helfrich model is incapable of explaining vesiculation if the coating area of proteins is relatively small. Anisotropic spontaneous curvatures based on the extended Helfrich model are needed to drive membrane fission. Depending on the type of anisotropic curvatures, the membrane tube could undergo tubular or hourglass necking. Furthermore, we suggest an experimental method to distinguish the type of anisotropic curvatures of a protein by comparing the force to maintain the membrane in a tubular shape in the presence and absence of the proteins.

ACKNOWLEDGMENTS

We acknowledge financial support from the National Natural Science Foundation of China under Grants No. 12147142, No. 11974292, No. 12174323, and No. 12004317; Fundamental Research Funds for Central Universities of China under Grant No. 20720200072 (RM); and 111 Project No. B16029.

APPENDIX A: DERIVATION OF THE MEMBRANE SHAPE EQUATIONS

Here, we show how to obtain the shape equations via the variational methods. The variation of the functional G_{tot} in Eq. (12) reads

$$\frac{\delta G_{\mathrm{tot}}}{2\pi} = \int_0^S ds\Bigg[\left(\frac{\partial\mathcal{L}}{\partial\psi} - \frac{d}{ds}\frac{\partial\mathcal{L}}{\partial\dot{\psi}}\right)\delta\psi + \left(\frac{\partial\mathcal{L}}{\partial r} - \frac{d}{ds}\frac{\partial\mathcal{L}}{\partial\dot{r}}\right)\delta r + \left(\frac{\partial\mathcal{L}}{\partial z} - \frac{d}{ds}\frac{\partial\mathcal{L}}{\partial\dot{z}}\right)\delta z + \left(\frac{\partial\mathcal{L}}{\partial a} - \frac{d}{ds}\frac{\partial\mathcal{L}}{\partial\dot{a}}\right)\delta a + \frac{\partial\mathcal{L}}{\partial\alpha}\delta\alpha + \frac{\partial\mathcal{L}}{\partial\beta}\delta\beta + \frac{\partial\mathcal{L}}{\partial\lambda}\delta\lambda\Bigg] + \frac{\partial\mathcal{L}}{\partial\dot{\psi}}\delta\psi|_{s=0}^{s=S} + \frac{\partial\mathcal{L}}{\partial\dot{r}}\delta r|_{s=0}^{s=S} + \frac{\partial\mathcal{L}}{\partial\dot{z}}\delta z|_{s=0}^{s=S}, \tag{A1}$$

which contains both the bulk terms (the terms in the square bracket) and the boundary terms (last three terms). A set of Euler-Lagrange equations can be obtained by the vanishing bulk terms, which are reduced to

$$\ddot{\psi} = \left(c_0^1 - c_0^2\right)\frac{\cos\psi}{r} + \frac{\sin\psi\cos\psi}{r^2} - \frac{f\cos\psi}{2\pi\kappa r} + \frac{pr\cos\psi}{2\kappa} + \frac{\alpha\sin\psi}{\kappa r} + \frac{\beta\cos\psi}{\kappa r} + \left(c_0^2 - c_0^1\right)\frac{\kappa_{12}\cos\psi}{\kappa r} + \dot{c_0^1} + \dot{c_0^2}\frac{\kappa_{12}}{\kappa} + c_0^1\frac{\dot{\kappa}}{\kappa} + c_0^2\frac{\dot{\kappa_{12}}}{\kappa} - \frac{\dot{\kappa_{12}}\sin\psi}{\kappa r} - \frac{\dot{\psi}\cos\psi}{r} - \dot{\psi}\frac{\dot{\kappa}}{\kappa}, \tag{A2}$$

$$\dot{\alpha} = pr\sin\psi + \frac{\kappa}{2}\left[\left(c_0^1\right)^2 + \left(c_0^2\right)^2\right] - \frac{\kappa\sin^2\psi}{2r^2} + \kappa_{12}c_0^1c_0^2 - \lambda - c_0^1\kappa\dot{\psi} - c_0^2\kappa_{12}\dot{\psi} + \frac{\kappa}{2}\dot{\psi}^2, \tag{A3}$$

$$\dot{\beta} = 0, \tag{A4}$$

$$\dot{\lambda} = \frac{\dot{\kappa}}{2}\left(c_1 - c_0^1\right)^2 + \frac{\dot{\kappa}}{2}\left(c_2 - c_0^2\right)^2 + \dot{\kappa_{12}}\left(c_1 - c_0^1\right)\left(c_2 - c_0^2\right) - \kappa\dot{c_0^1}\left(c_1 - c_0^1\right) - \kappa\dot{c_0^2}\left(c_2 - c_0^2\right) - \kappa_{12}\dot{c_0^2}\left(c_1 - c_0^1\right) - \kappa_{12}\dot{c_0^1}\left(c_2 - c_0^2\right), \tag{A5}$$

$$\dot{r} = \cos\psi, \tag{A6}$$

$$\dot{z} = -\sin\psi, \tag{A7}$$

$$\dot{a} = r. \tag{A8}$$

It should be noted that a denotes the area of the membrane calculated from the tip, and the prefactor 2π in front of r in Eq. (A8) is neglected.

So far, we have derived seven equations, Eqs. (A2)–(A8), which are all first order except Eq. (A2), which is second order with respect to ψ. In addition, the total arc length S is an unknown parameter. Therefore, a total number of nine boundary conditions (BCs) are needed to close the problem. To obtain the BCs, we set the boundary terms in Eq. (A1) to zero. At the membrane tip ($s = 0$), we have

$$\psi(s=0) = 0,\ r(s=0) = 0,\ \beta(s=0) = 0,\ a(s=0) = 0. \tag{A9}$$

At the base of the membrane ($s = S$), we impose

$$z(s=S) = 0, \quad r(s=S) = R_b, \quad \sigma(s=S) = \sigma_0. \tag{A10}$$

As for the angle $\psi(s = S)$ at the boundary, we allow it to freely rotate. This implicates the free-hinge BC:

$$\frac{\partial\mathcal{L}}{\partial\dot{\psi}} = \left[\kappa\left(c_1 - c_0^1\right) + \kappa_{12}\left(c_2 - c_0^2\right)\right]\Big|_{s=S} = 0. \tag{A11}$$

To complete the BCs, we construct the effective Hamiltonian:

$$\mathcal{H} = \mathcal{L} - \dot{\psi}\frac{\partial\mathcal{L}}{\partial\dot{\psi}} - \dot{r}\frac{\partial\mathcal{L}}{\partial\dot{r}} - \dot{z}\frac{\partial\mathcal{L}}{\partial\dot{z}} - \dot{a}\frac{\partial\mathcal{L}}{\partial\dot{a}}. \tag{A12}$$

It is easy to prove that $\mathcal{H}$ is conserved along the arc length, i.e., $\mathcal{H}(s) = 0$. We therefore impose the ninth BC:

$$\mathcal{H}(s=0) = 0. \tag{A13}$$

The seven equations, Eqs. (A2)–(A8), and one unknown parameter S together with the nine BCs, Eqs. (A9)–(A11) and (A13), constitute a well-defined boundary value problem of ordinary differential equations.

APPENDIX B: PHASE DIAGRAM OF THE HELFRICH MODEL WITH VARIED COATING AREA

We have shown that, if the coating area of BAR proteins is $<2000\,\mathrm{nm}^2$, increasing the spontaneous curvature in the Helfrich model ($\kappa_{12} = \kappa$) cannot form a narrow enough neck to trigger vesiculation. Here, we study the effect of the coating area on the neck morphology for the Helfrich model, which is shown in Fig. 9. We find that, if the coating area is $>2000\,\mathrm{nm}^2$, increasing the spontaneous curvature c_0^2 can also reduce the neck radius $<5\,\mathrm{nm}$ [Fig. 9(a)]. For large c_0^2, the neck becomes pearl shaped with multiple undulations, and the neck ra-

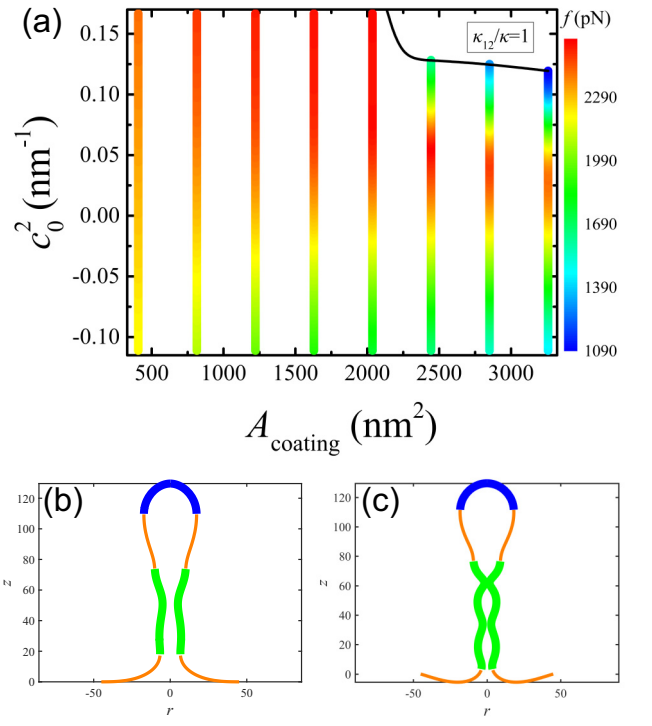

FIG. 9. (a) A two-dimensional phase diagram on the (c_0^2-A_{coating}) plane characterizes the interrelated effects of the spontaneous curvature c_0^2 and the coating area A_{coating} on the formation of vesicles. The colored region represents the membrane shapes that have not undergone vesiculation with a color code demonstrating the force magnitude to maintain the membrane at a certain height. The white regions represent the membrane shapes that have a necking radius smaller than the critical value of 5 nm, by which a vesiculation is regarded to occur. The coupling constant κ_{12} equals κ. Profile views of membrane morphologies for the neck radius close to (b) 5 nm and (c) <5 nm.

dius can be much smaller than 5 nm [Figs. 9(b) and 9(c)], which is like the infinitesimal radius studied in previous works [26,27].

APPENDIX C: NECK MORPHOLOGY FOR AN ELONGATED TUBULAR MEMBRANE

In the main text, we consider a tubular membrane of which the tip is coated with clathrins that generate isotropic spontaneous curvature, and the side is coated with BAR proteins that generate anisotropic spontaneous curvature. To test whether our results about the anisotropic proteins at the side of the tubular membrane are influenced by the isotropic proteins at the membrane tip, we pull the membrane to a height of 540 nm and coat the anisotropic proteins at a position between 250 and 300 nm. When comparing with the original results for which the membrane is fixed to a height of 130 nm, we find only a minor quantitative difference (Fig. 10). Therefore, our results about the anisotropic proteins are independent of the particular geometry we have used in the main text.

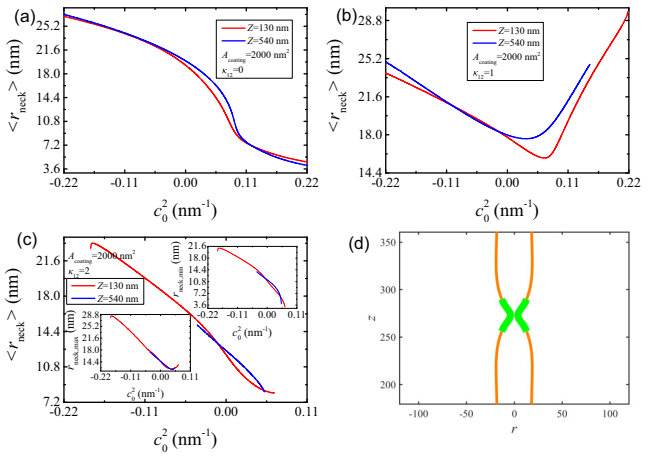

FIG. 10. The mean value of the neck radius $\langle r_{\text{neck}} \rangle$ as a function of the spontaneous curvature c_0^2 for (a) $\kappa_{12} = 0$, (b) $\kappa_{12} = 1$, and (c) $\kappa_{12} = 2$. The average is taken over the protein-coated area at the side of the membrane. (d) Profile views of membrane morphologies for positive spontaneous curvature c_0^2 when $\kappa_{12} = 2$ and the membrane height is $Z = 540$ nm.

[1] W. Kukulski, M. Schorb, M. Kaksonen, and J. A. G. Briggs, Plasma membrane reshaping during endocytosis is revealed by time-resolved electron tomography, Cell **150**, 508 (2012).

[2] J. S. Bonifacino and B. S. Glick, The mechanisms of vesicle budding and fusion, Cell **116**, 153 (2004).

[3] T. Kishimoto, Y. Sun, C. Buser, J. Liu, A. Michelot, and D. G. Drubin, Determinants of endocytic membrane geometry, stability, and scission, Proc. Natl. Acad. Sci. USA **108**, E979-E988 (2011).

[4] M. J. Taylor, D. Perrais, and C. J. Merrifield, A high precision survey of the molecular dynamics of mammalian clathrinmediated endocytosis, PLoS Biol. **9**, e1000604 (2011).

[5] A. Mahapatra, C. Uysalel, and P. Rangamani, The mechanics and thermodynamics of tubule formation in biological membranes, J. Membr. Biol. **254**, 273 (2021).

[6] D. Perrais and C. J. Merrifield, Dynamics of endocytic vesicle creation, Dev. Cell **9**, 581 (2005).

[7] H. T. McMahon and E. Boucrot, Molecular mechanism and physiological functions of clathrin-mediated endocytosis, Nat. Rev. Mol. Cell Biol. **12**, 517 (2011).

[8] O. Avinoam, M. Schorb, C. J. Beese, J. A. G. Briggs, and M. Kaksonen, Endocytic sites mature by continuous bending and remodeling of the clathrin coat, Science **348**, 1369 (2015).

[9] G. Kumar and A. Sain, Shape transitions during clathrininduced endocytosis, Phys. Rev. E **94**, 062404 (2016).

[10] D. Bucher, F. Frey, K. A. Sochacki, S. Kummer, J. P. Bergeest, W. J. Godinez, H. G. Kräusslich, K. Rohr, J. W. Taraska, U. S. Schwarz *et al.*, Clathrin-adaptor ratio and membrane tension regulate the flat-to curved transition of the clathrin coat during endocytosis, Nat. Commun. **9**, 1109 (2018).

[11] Z. Chen and S. L. Schmid, Evolving models for assembling and shaping clathrin-coated pits, J. Cell Biol. **219**, e202005126 (2020).

[12] C. T. Lee, M. Akamatsu, and P. Rangamani, Value of models for membrane budding, Curr. Opin. Cell Biol. **71**, 38 (2021).

[13] M. Simunovic, G. A. Voth, A. Callan-Jones, and P. Bassereau, When physics takes over: BAR proteins and membrane curvature, Trends Cell Biol. **25**, 780 (2015).

[14] M. Simunovic, C. Prévost, A. Callan-Jones, and P. Bassereau, Physical basis of some membrane shaping mechanisms, Phil. Trans. R. Soc. A. **374**, 20160034 (2016).

[15] A. Frost, R. Perera, A. Roux, K. Spasov, O. Destaing, E. H. Egelman, P. De Camilli, and V. M. Unger, Structural basis of membrane invagination by F-BAR domains, Cell **132**, 807 (2008).

[16] B. Habermann, The BAR-domain family of proteins: a case of bending and binding? EMBO Rep. **5**, 250 (2004).

[17] C. Mim, H. Cui, J. A. Gawronski-Salerno, A. Frost, E. Lyman, G. A. Voth, and V. M. Unger, Structural basis of membrane bending by the N-BAR protein endophilin, Cell **149**, 137 (2012).

[18] N. Walani, J. Torres, and A. Agrawal, Endocytic proteins drive vesicle growth via instability in high membrane tension environment, Proc. Natl. Acad. Sci. USA **112**, E1423 (2015).

[19] J. Agudo-Canalejo and R. Lipowsky, Stabilization of membrane necks by adhesive particles, substrate surfaces, and constriction forces, Soft Matter **12**, 8155 (2016).

[20] J. Steinkühler, R. L. Knorr, Z. Zhao, T. Bhatia, S. M. Bartelt, S. Wegner, R. Dimova, and R. Lipowsky, Controlled division of cell-sized vesicles by low densities of membrane-bound proteins, Nat. Commun. **11**, 905 (2020).

[21] A.-L. Le Roux, C. Tozzi, N. Walani, X. Quiroga, D. Zalvidea, X. Trepat, M. Staykova, M. Arroyo, and P. Roca-Cusachs, Dynamic mechanochemical feedback between curved membranes and BAR protein self-organization, Nat. Commun. **12**, 6550 (2021).

[22] F. Yuan, H. Alimohamadi, B. Bakka, A. N. Trementozzi, K. J. Day, N. L. Fawzi, P. Rangamani, and J. C. Stachowiak, Membrane bending by protein phase separation, Proc. Natl. Acad. Sci. USA **118**, e2017435118 (2021).

[23] M. Chabanon and P. Rangamani, Gaussian curvature directs the distribution of spontaneous curvature on bilayer membrane necks, Soft Matter **14**, 2281 (2018).
[24] H. Alimohamadi, R. Vasan, J. E. Hassinger, J. C. Stachowiak, and P. Rangamani, The role of traction in membrane curvature generation, Mol. Biol. Cell **29**, 2024 (2018).
[25] U. Seifert, K. Berndl, and R. Lipowsky, Shape transformations of vesicles: Phase diagram for spontaneouscurvature and bilayer-coupling models, Phys. Rev. A **44**, 1182 (1991).
[26] B. Fourcade, L. Miao, M. Rao, M. Wortis, and R. K. P. Zia, Scaling analysis of narrow necks in curvature models of fluid lipid-bilayer vesicles, Phys. Rev. E **49**, 5276 (1994).
[27] L. Miao, B. Fourcade, M. Rao, M. Wortis, and R. K. P. Zia, Equilibrium budding and vesiculation in the curvature model of fluid lipid vesicles, Phys. Rev. A **43**, 6843 (1991).
[28] F. Jülicher and R. Lipowsky, Domain-Induced Budding of Vesicles, Phys. Rev. Lett. **70**, 2964 (1993).
[29] F. Jülicher and R. Lipowsky, Shape transformations of vesicles with intramembrane domains, Phys. Rev. E **53**, 2670 (1996).
[30] A. F. Loftus, V. L. Hsieh, and R. Parthasarathy, Modulation of membrane rigidity by the human vesicle trafficking proteins Sar1A and Sar1B, Biochem. Biophys. Res. Commun. **426**, 585 (2012).
[31] I. Tsafrir, D. Sagi, T. Arzi, M. A. Guedeau-Boudeville, V. Frette, D. Kandel, and J. Stavans, Pearling Instabilities of Membrane Tubes with Anchored Polymers, Phys. Rev. Lett. **86**, 1138 (2001).
[32] T. F. Roth and K. R. Porter, Yolk protein uptake in the oocyte of the mosquito *Aedes aegypti. L*, J. Cell Biol. **20**, 313 (1964).
[33] R. G. W. Anderson, M. S. Brown, and J. L. Goldstein, Role of the coated endocytic vesicle in the uptake of receptor-bound low density lipoprotein in human fibroblasts, Cell **10**, 351 (1977).
[34] J. Heuser, Three-dimensional visualization of coated vesicle formation in fibroblasts, J. Cell Biol. **84**, 560 (1980).
[35] J. C. Stachowiak, F. M. Brodsky, and E. A. Miller, A cost-benefit analysis of the physical mechanisms of membrane curvature, Nat. Cell Biol. **15**, 1019 (2013).
[36] M. Pinot, S. Vanni, S. Pagnotta, S. Lacas-Gervais, L. Payet, T. Ferreira, R. Gautier, B. Goud, B. Antonny, and H. Barelli, Polyunsaturated phospholipids facilitate membrane deformation and fission by endocytic proteins, Science **345**, 693 (2014).
[37] Z. Shi and T. Baumgart, Membrane tension and peripheral protein density mediate membrane shape transitions, Nat. Commun. **6**, 5974 (2014).
[38] A. Diz-Muñoz, D. A. Fletcher, O. D. Weiner, Use the force: Membrane tension as an organizer of cell shape and motility, Trends Cell Biol. **23**, 47 (2013).
[39] P. J. Wen, S. Grenklo, G. Arpino, X. Tan, H. Liao, J. Heureaux, S. Peng, H. Chiang, E. Hamid, W. Zhao *et al.*, Actin dynamics provides membrane tension to merge fusing vesicles into the plasma membrane, Nat. Commun. **7**, 12604 (2016).
[40] M. G. J. Ford, I. G. Mills, B. J. Peter, Y. Vallis, G. J. K. Praefcke, P. R. Evans, and H. T. McMahon, Curvature of clathrin-coated pits driven by epsin, Nature (London) **419**, 361 (2002).
[41] J. C. Stachowiak, E. M. Schmid, C. J. Ryan, H. S. Ann, D. Y. Sasaki, M. B. Sherman, P. L. Geissler, D. A. Fletcher, and C. C. Hayden, Membrane bending by protein-protein crowding, Nat. Cell Biol. **14**, 944 (2012).
[42] D. J. Busch, J. R. Houser, C. C. Hayden, M. B. Sherman, E. M. Lafer, and J. C. Stachowiak, Intrinsically disordered proteins drive membrane curvature, Nat. Commun. **6**, 7875 (2015).
[43] R. Lipowsky, Spontaneous tubulation of membranes and vesicles reveals membrane tension generated by spontaneous curvature, Faraday Discuss. **161**, 305 (2013).
[44] P. Sens and M. S. Turner, Theoretical model for the formation of caveolae and similar membrane invaginations, Biophys. J. **86**, 2049 (2004).
[45] J. Liu, M. Kaksonen, D. G. Drubin, and G. Oster, Endocytic vesicle scission by lipid phase boundary forces, Proc. Natl. Acad. Sci. USA **103**, 10277 (2006).
[46] T. Zhang, R. Sknepnek, M. J. Bowick, and J. M. Schwarz, On the modeling of endocytosis in yeast, Biophys. J. **108**, 508 (2015).
[47] J. E. Hassinger, G. Oster, D. G. Drubin, and P. Rangamani, Design principles for robust vesiculation in clathrin-mediated endocytosis, Proc. Natl. Acad. Sci. USA **114**, E1118-E1127 (2017).
[48] R. Ma and J. Berro, Endocytosis against high turgor pressure is made easier by partial coating and freely rotating base, Biophys. J. **120**, 1625 (2021).
[49] D. Kabaso, N. Bobrovska, W. Góźdź, N. Gov, V. Kralj-Iglič, P. Veranič, and A. Iglič, On the role of membrane anisotropy and BAR proteins in the stability of tubular membrane structures, J. Biomech. **45**, 231 (2012).
[50] A. Iglič, B. Babnik, U. Gimsa, and V. Kralj-Iglič, On the role of membrane anisotropy in the beading transition of undulated tubular membrane structures, J. Phys. A: Math. Gen. **38**, 8527 (2005).
[51] N. Bobrovska, W. Góźdź, V. Kralj-Iglič, and A. Iglič, On the role of anisotropy of membrane components in formation and stabilization of tubular structures in multicomponent membranes, PLoS ONE **8**, e73941 (2013).
[52] N. Walani, J. Torres, and A. Agrawal, Anisotropic spontaneous curvatures in lipid membranes, Phys. Rev. E **89**, 062715 (2014).
[53] D. Menon, D. Hummel, and M. Kaksonen, Mathematical modeling of endocytic actin patch kinetics in fission yeast: disassembly requires release of actin filament fragments, Mol. Biol. Cell. **33**, ar114 (2022).
[54] J. Berro, V. Sirotkin, and T. D. Pollard, Regulation of membrane scission in yeast endocytosis, Mol. Biol. Cell. **21**, 2905 (2010).